Critical Evaluation of the Thermometric Performance of Ratiometric Luminescence Thermometers based on $Ba_3(VO_4)_2$:Mn^{5+}, Nd^{3+} for Deep-Tissue Thermal Imaging

W. M. Piotrowski[1]*, R. Marin[2,3], M. Szymczak[1], E. Martín Rodríguez[4,5], D. H. Ortgies[2,3,5], P. Rodríguez-Sevilla[2,5], P. Bolek[6], M. D. Dramićanin[7], D. Jaque[2,3,5], L. Marciniak[1]*

[1]Institute of Low Temperature and Structure Research, Polish Academy of Sciences, Okólna 2, 50-422 Wroclaw, Poland

[2]Nanomaterials for Bioimaging Group (nanoBIG), Departamento de Física de Materiales, Facultad de Ciencias, Universidad Autónoma de Madrid, C/ Francisco Tomás y Valiente 7, 28049 Madrid, Spain

[3] Institute for Advanced Research in Chemistry (IAdChem), Campus de Cantoblanco, 28049 Madrid, Spain

[4]Nanomaterials for Bioimaging Group (nanoBIG), Departamento de Física Aplicada, Facultad de Ciencias, Universidad Autónoma de Madrid, C/ Francisco Tomás y Valiente 7, 28049 Madrid, Spain

[5] Nanomaterials for Bioimaging Group (nanoBIG), Instituto Ramón y Cajal de Investigación Sanitaria (IRYCIS), Hospital Ramón y Cajal, Ctra. De Colmenar Viejo km 9.100, 28034 Madrid, Spain

[6] Faculty of Chemistry, University of Wrocław14 F. Joliot-Curie, Wrocław 50-383, Poland

[7] Centre of Excellence for Photoconversion, Vinča Institute of Nuclear Sciences – National Institute of the Republic of Serbia, University of Belgrade, P.O. Box 522, Belgrade 11001, Serbia

* corresponding author: w.piotrowski@intibs.pl, l.marciniak@intibs.pl

KEYWORDS luminescence thermometry, thermal imaging, manganese, neodymium, $Ba_3(VO_4)_2$, NIR spectral range

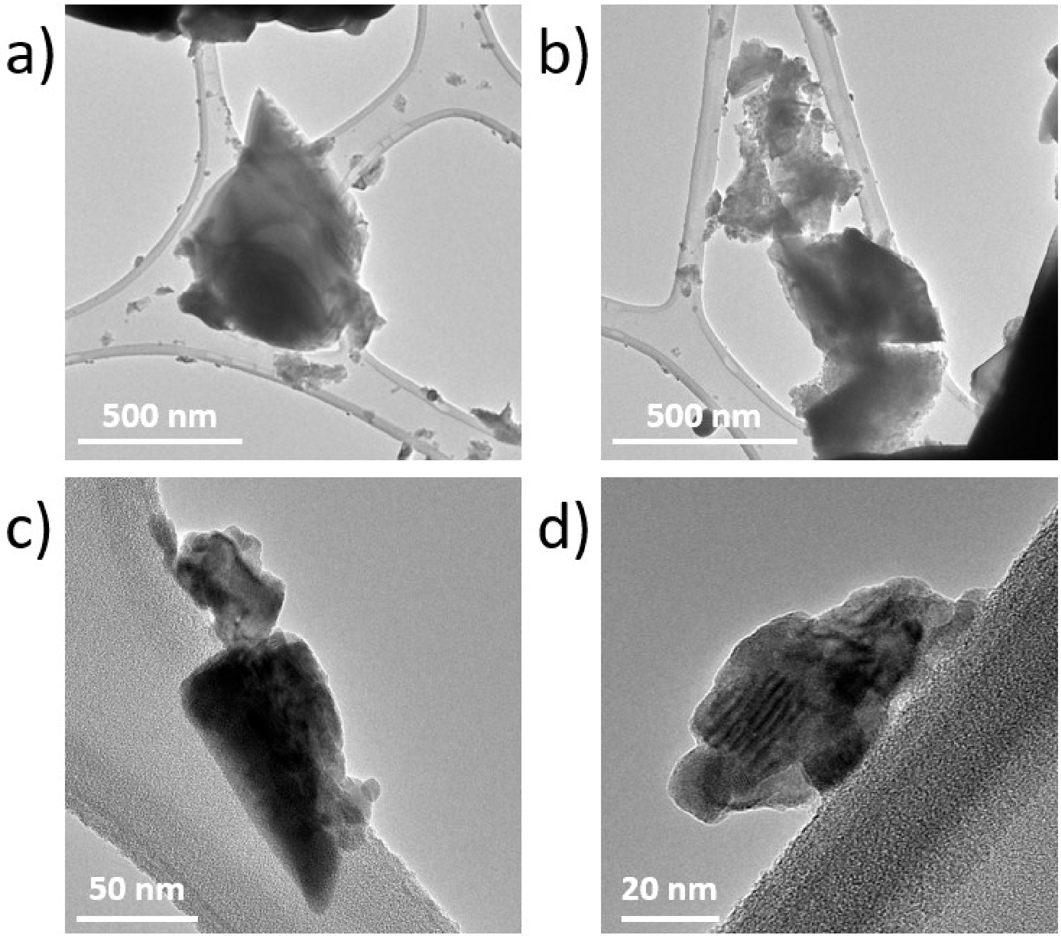

Figure S1. Representative TEM images of $Ba_3(VO_4)_2$:0.1% Mn^{5+}, 5% Nd^{3+} materials.

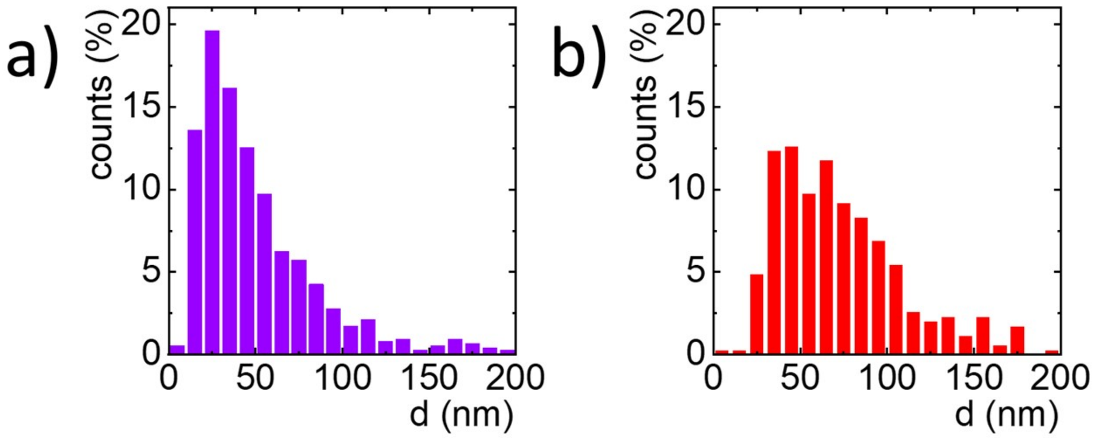

Figure S2. Particle size distributions for $Ba_3(VO_4)_2$:0.1% Mn^{5+}, 0.1% Nd^{3+} – a) and $Ba_3(VO_4)_2$:0.1% Mn^{5+}, 5% Nd^{3+} powder – b).

Table S1. The elemental analysis of the $Ba_3(VO_4)_2$: 0.1% Mn^{5+}, y% Nd^{3+}

		0.1% Mn, 0.1% Nd	0.1% Mn, 0.2% Nd	0.1% Mn, 0.5% Nd	0.1% Mn, 1% Nd	0.1% Mn, 2% Nd	0.1% Mn, 5% Nd
Ba 233.527 {445}	concentration (mg/l)	299.563	294.333	212.391	291.982	285.517	295.093
Ba 230.424 {446}		303.749	295.945	213.635	295.773	289.453	299.646
	Ba content (%)	**78.564±0.545**	**78.469±0.214**	**78.520±0.229**	**77.448±0.500**	**76.805±0.526**	**74.086±0.567**
V 309.311 {109}	concentration (mg/l)	82.839	81.374	57.631	82.138	80.884	85.96
V 292.402 {115}		80.832	79.163	56.22	80.401	79.167	84.202
	V content (%)	**21.313±0.261**	**21.341±0.294**	**20.984±0.260**	**21.418±0.229**	**21.380±0.229**	**21.197±0.219**
Mn 257.610 {131}	concentration (mg/l)	0.114	0.086	0.061	0.084	0.140	0.099
Mn 260.569 {129}		0.121	0.094	0.066	0.089	0.147	0.107
	Mn content (%)	**0.031±0.0009**	**0.024±0.0011**	**0.023±0.0009**	**0.023±0.0007**	**0.038±0.0009**	**0.026±0.0010**
Nd 401.225 {84}	concentration (mg/l)	0.342	0.600	1.253	4.145	6.531	18.483
Nd 406.109 {83}		0.368	0.653	1.316	4.292	6.770	19.177
	Nd content (%)	**0.092±0.0034**	**0.167±0.0070**	**0.473±0.0116**	**1.112±0.0194**	**1.777±0.0319**	**4.691±0.0865**

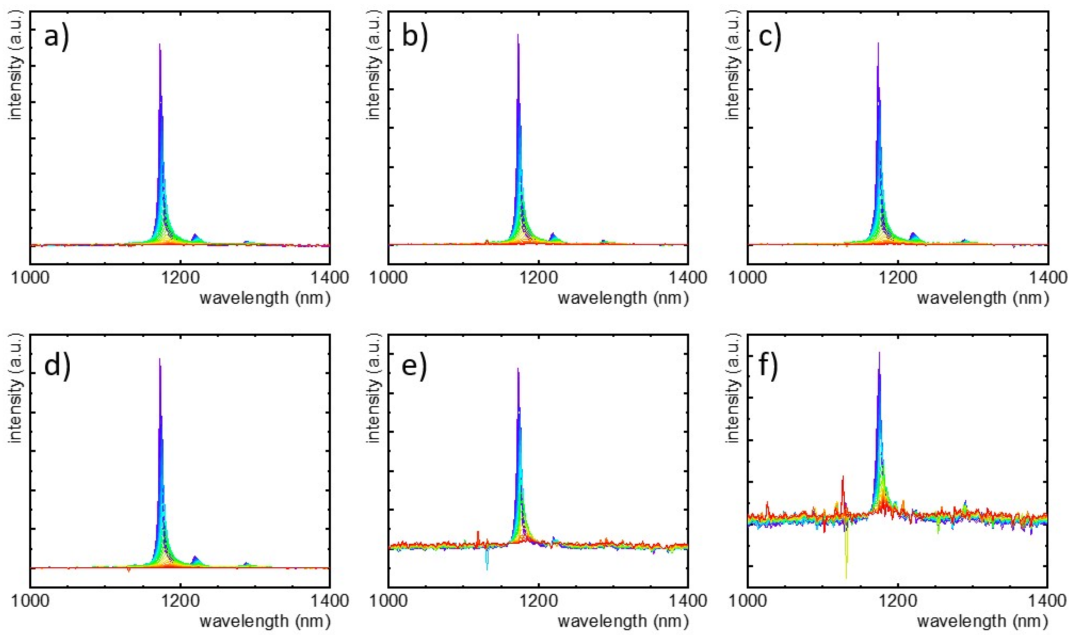

Figure S3. Thermal evolution of emission spectra of $Ba_3(VO_4)_2$:1% Mn^{5+}, y% Nd^{3+}, where y = 0.1 – a); 0.5 – b); 1 – c); 2 – d); 5 – e); 10 – f).

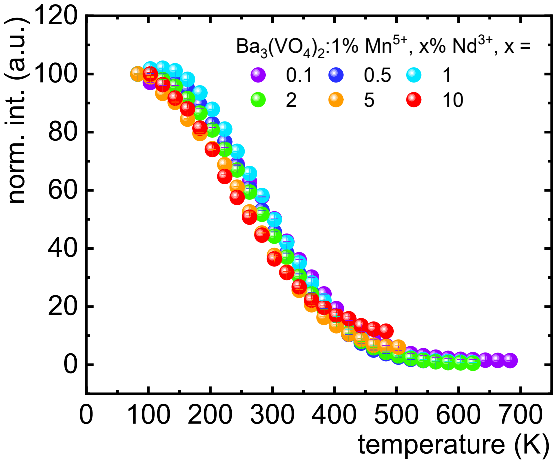

Figure S4. Thermal evolution of the normalized intensity of Mn^{5+} emission band for $Ba_3(VO_4)_2$: 1% Mn^{5+}, y% Nd^{3+} with different Nd^{3+} concentration.

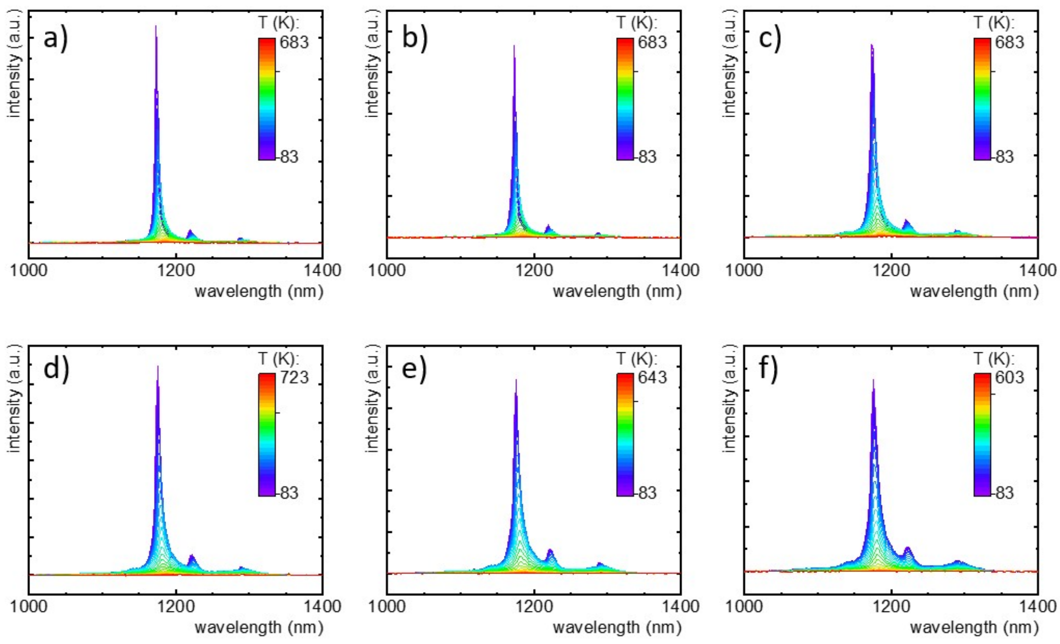

Figure S5. Thermal evolution of emission spectra of $Ba_3(VO_4)_2$:x% Mn^{5+}, where x = 0.1 – a); 0.2 – b); 0.5 – c); 1 – d); 2 – e); 5 – f).

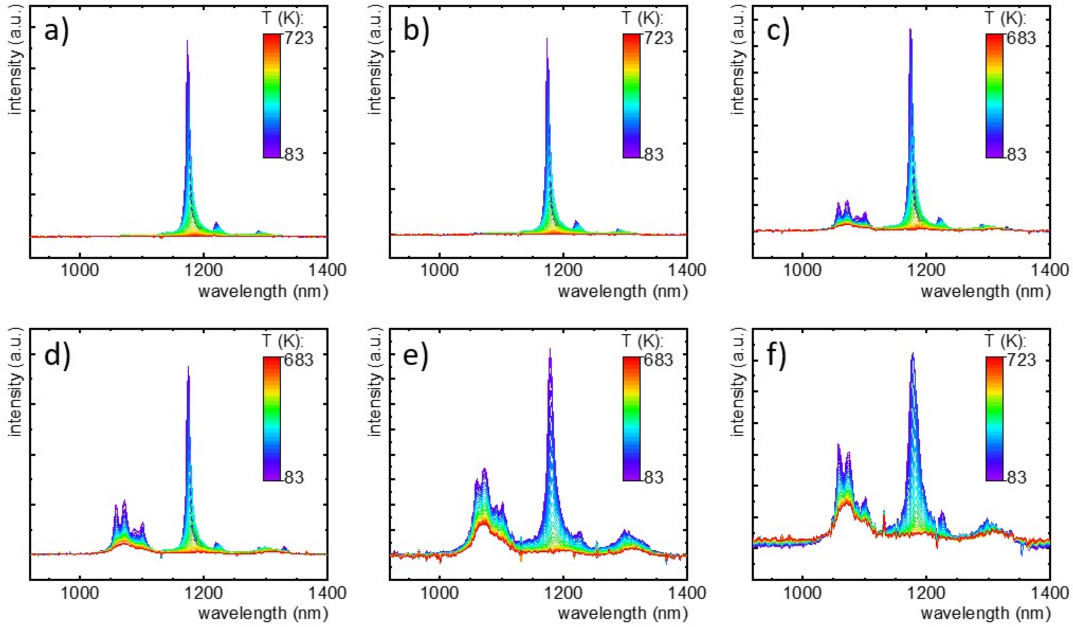

Figure S6. Thermal evolution of emission spectra of $Ba_3(VO_4)_2$:0.1% Mn^{5+}, y% Nd^{3+}, where y = 0.1 – a); 0.2 – b); 0.5 – c); 1 – d); 2 – e); 5 – f).

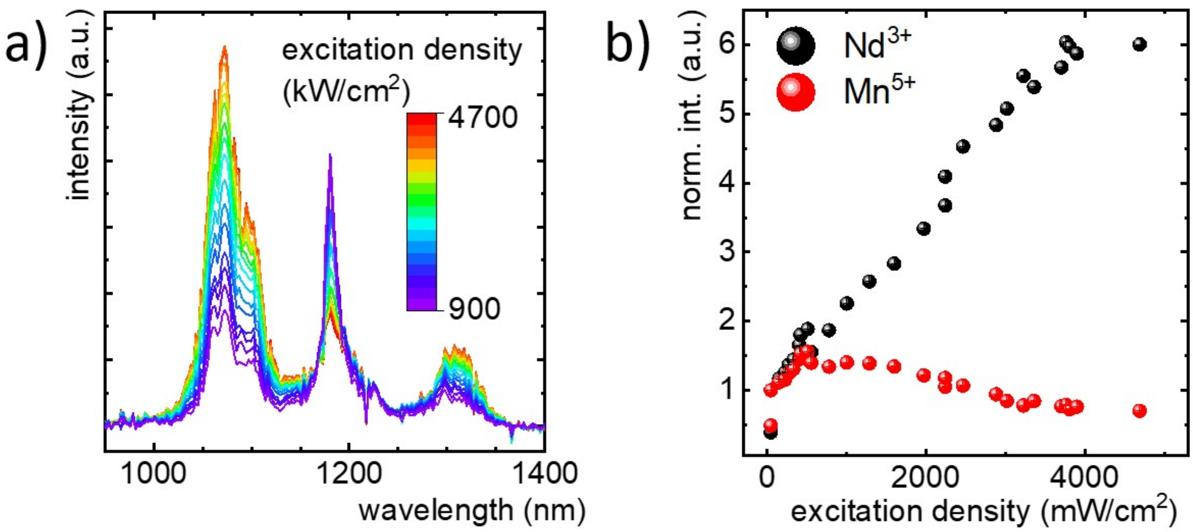

Figure S7. Emission spectra of $Ba_3(VO_4)_2$:0.1% Mn^{5+}, 2% Nd^{3+} with different excitation density λ_{exc} = 808 nm – a) and normalized intensity of Mn^{5+} (λ_{em} = 1180 nm) and Nd^{3+} bands (λ_{em} = 1070 nm) in the function of excitation density – b).

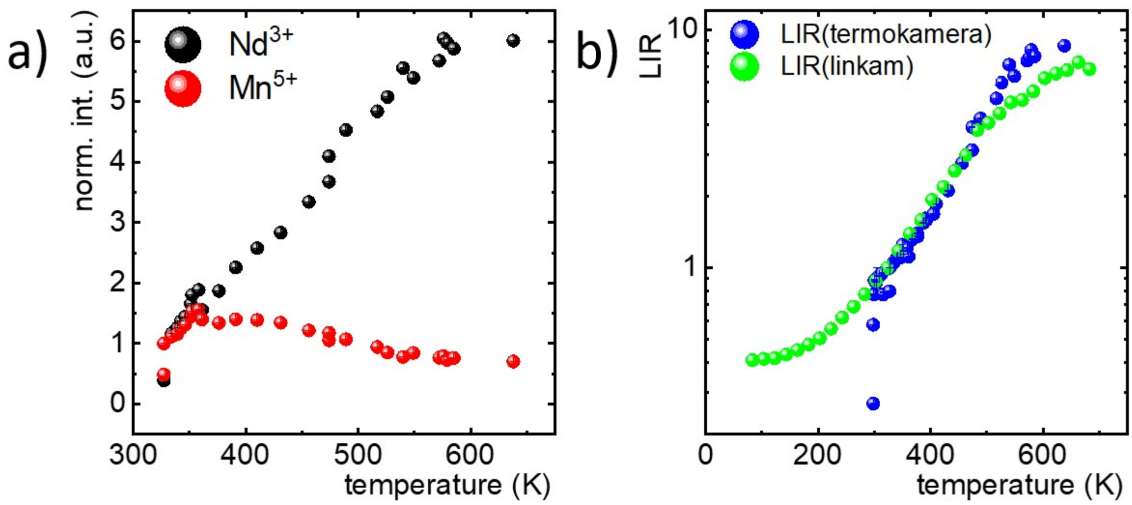

Figure S8. Normalized intensity of Mn^{5+} (λ_{em} = 1180 nm) and Nd^{3+} bands (λ_{em} = 1070 nm) in the function of temperature detected by thermal camera – a) and comparison of LIR values in the function of temperature controlled by Linkam and detected by thermal camera when the samples was heated by laser – b).

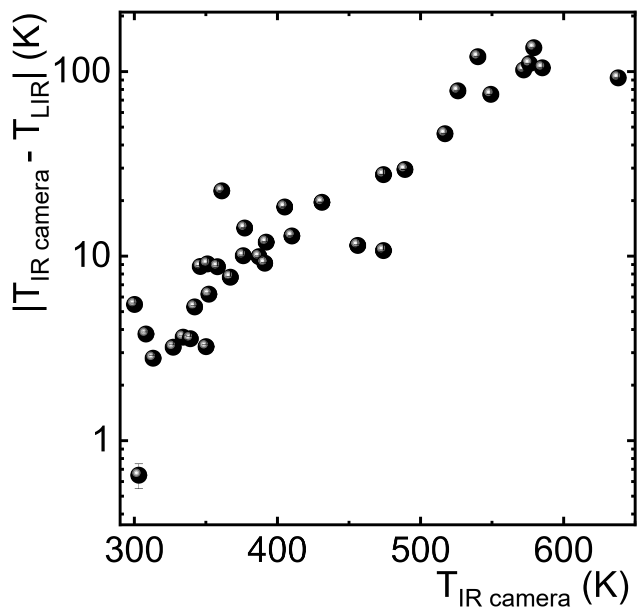

Figure S9. The plot of difference between IR camera and LIR temperature readout vs temperature controlled by IR camera.

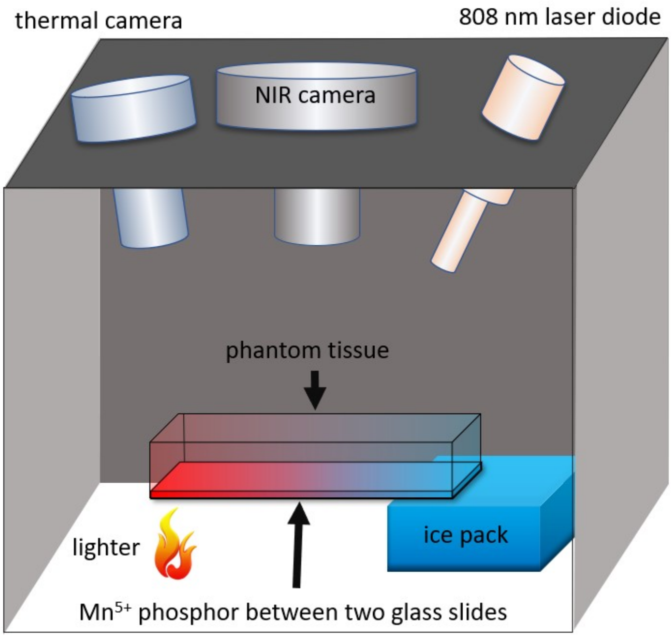

Figure S10. The schematic presentation of a thermal imaging measurement system based on a ratiometric approach.

Figure S11. the photo of tissue phantom B with the $Ba_3(VO_4)_2$:0.1% Mn^{5+}, 2% Nd^{3+}

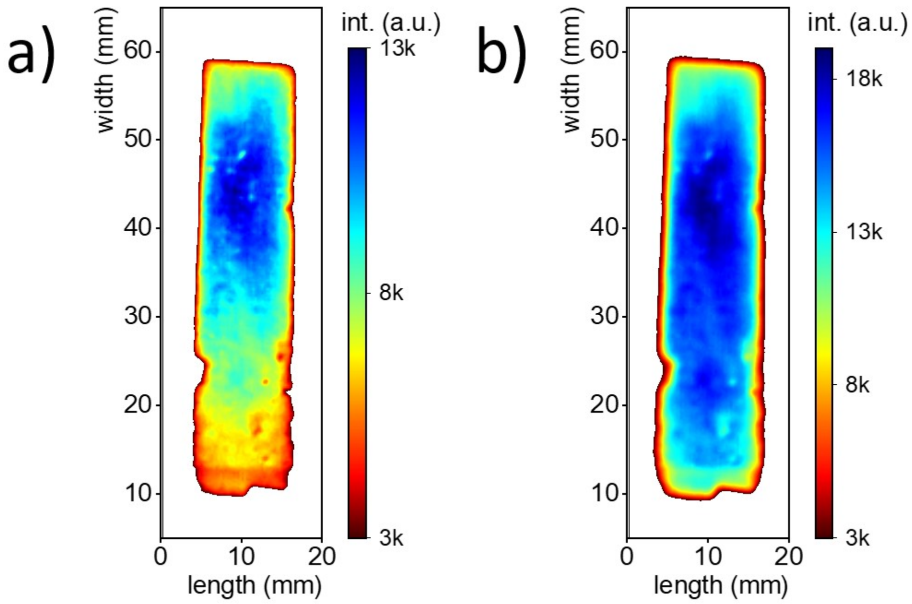

Figure S12. The maps of intensity obtained with 1200 nm bandpass filter – a) and 1150 nm shortpass filter – b) for $Ba_3(VO_4)_2$:0.1% Mn^{5+}, 2% Nd^{3+} phosphor through phantom tissue.

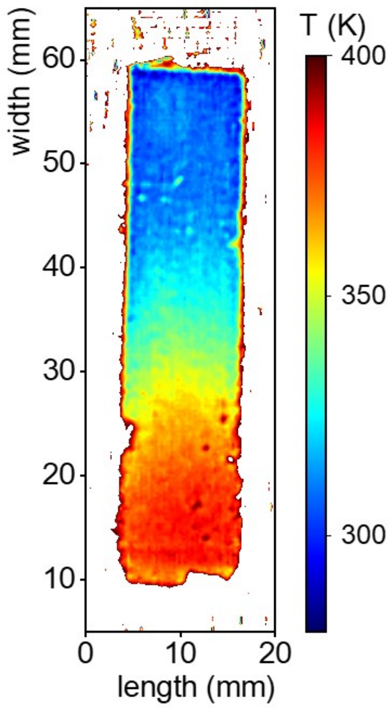

Figure S13. Temperature map with induced thermal gradient for $Ba_3(VO_4)_2$:0.1% Mn^{5+}, 2% Nd^{3+} phosphor obtained through phantom tissue.

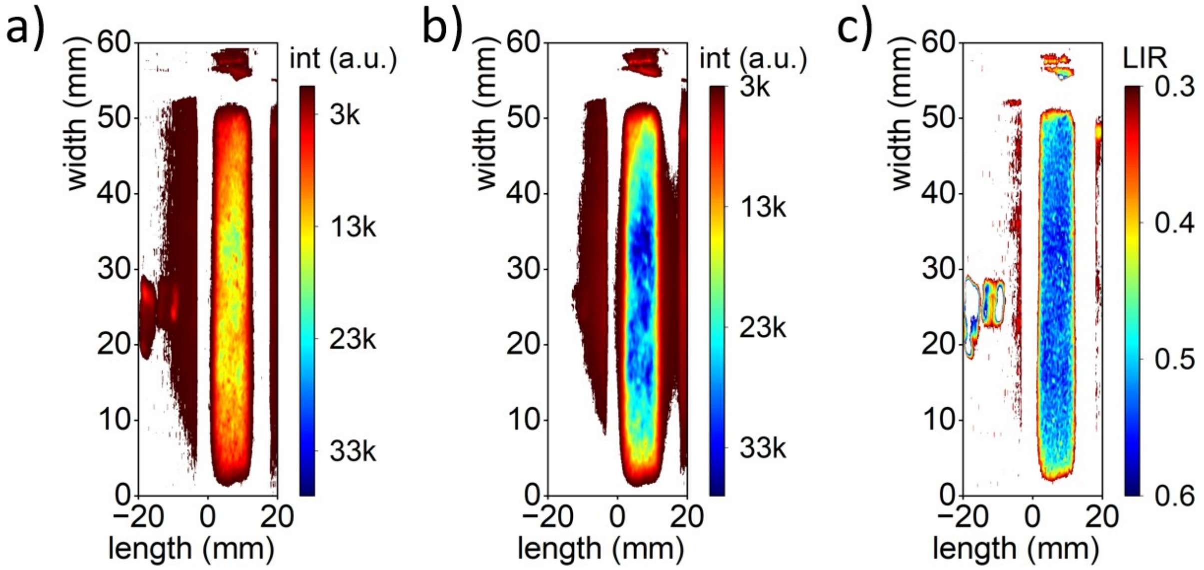

Figure S14. The maps of intensity obtained with 1200 nm bandpass filter – a) and 1150 nm shortpass filter – b) and LIR map – c) for $Ba_3(VO_4)_2$:0.1% Mn^{5+}, 2% Nd^{3+} phosphor through phantom tissue with 0.1% of Indian ink.